The International Journal of Advanced Manufacturing Technology (2019) 102:4273–4287
https://doi.org/10.1007/s00170-019-03369-y

ORIGINAL ARTICLE

Global interference detection technology for five-axis machining of complex surfaces

Juan Du[1] · Pengcheng Liu[1] · Hongying Zhi[1] · Peng Ding[1]

Received: 31 August 2018 / Accepted: 20 January 2019 / Published online: 8 March 2019

Abstract
Global interference detection and avoidance are key issues in tool path planning for five-axis machining of complex surfaces. Improving the detection accuracy and efficiency has always been the main goal of global interference research. In this paper, a novel method for fast interference judgment is proposed. First, the four planes with X or Y extremum are obtained by the intersection operation between the plane and the machined surface and solving extremum, respectively. Then, the four boundaries of the initial interference detection area are obtained by intersecting the four extreme planes with the machined surface. To determine whether there is collision interference between the tool and the machined part, the shortest distance between the tool axis and the detection area is used for interference judgment. The shortest distance can be obtained by calculating the distance between the discrete point in the detection area and the tool axis. In order to ensure the uniformity of the discrete points, the discretization of points was carried out in the projection area of the initial detection area on the XOY plane, rather than on the part surface. For improving the efficiency of interference detection, the four-sided constraint method is used to screen the discrete points in the initial detection area. Only the points satisfying the screening conditions can be used as effective detection points to calculate the distances, and the shortest distance can be found from all the calculated distances. In this paper, the subdivision technology is used to achieve high-precision interference detection. At the end of the paper, the interference detection algorithm was tested by two examples, and the correctness of the test results was verified by the VERICUT simulation and cutting experiment. The proposed algorithm can be applied to interference detection of five-axis end milling of complex surfaces.

Keywords Five-axis machining · Interference detection · Fillet-end milling cutter

1 Introduction and literature review

Compared with the three-axis machine tools, the five-axis machine tools increase two degrees of freedom of rotation; so, the machining of complex surfaces can be carried out on five-axis machine tools. However, in the process of five-axis machining, unreasonable tool posture will cause global interference collision between the tool and workpiece or other parts of the machine tool, which leads to structural damage of the machine tools, endangering the safety of operators. Therefore, in order to avoid global interference, off-line interference detection and elimination should be carried out before complex surface milling.

✉ Hongying Zhi
lgzdj731010@sina.com

[1] Taiyuan University of Science and Technology, Taiyuan 030024, Shanxi, China

In this paper, global interference refers to the collision interference between the tool and the workpiece being processed. Figure 1 shows the global interference diagram of the five-axis machining of a complex surface by a fillet-end milling cutter.

A great deal of research on the global interference in multi-axis numerical control machining has been carried out by scholars at home and abroad [1–7]. The main methods of interference detection include distance calculation (vector)-based method [3, 8–10], convex hull-based method [11–14], discrete based method [15], and mapping and C space-based method [16–19]. Before planning the optimal measurement path, Lin and Chow used the distance method to determine whether there was contact or interference between the probe and the part to be measured [8]. Wang et al. developed a collision detection approach by using a combination of machining environment culling and a two-phase collision detection strategy [9]. Wang et al. proposed a method of collision-free machining fixture space design based on a parametric tool space for five-axis grinding [10]. The convex hull method adopts the convex hull

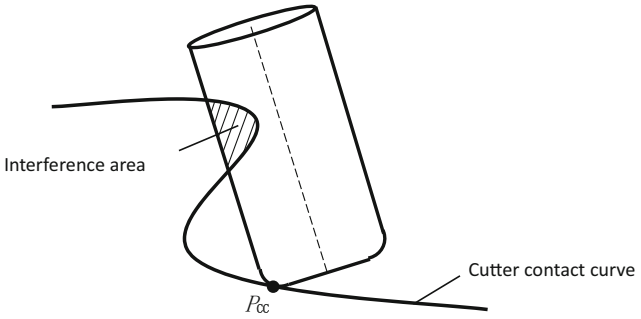

Fig. 1 Global interference diagram of five-axis machining

characteristics of Bezier, B-spline and NURBS (non-uniform rational B-spline) curves and surfaces for global interference detection. Lee et al. proposed a two-step method for global interference detection. First, the convex hull property of the surface is used to determine the possible area of interference of the cutter, and, then, accurate interference judgments are performed in the possible area [11]. Danaei et al. [15] used the principle of triangle intersection to check for interference. The cutter and the part surface were discretised into triangular patches. By evaluating the positional relationship between the two sets of triangles, the researcher analyzed and judged whether there is global interference between the cutter and the part surface. The principle of mapping method is to map the part's surface and the tool surface onto a two-dimensional plane or spherical surface for interference judgment. Tseng and Joshi [17] constructed an offset surface to convert the cutter radius to a machined surface and determined the feasible area of the cutter by coordinate rotation and transformation. Jimenez and Torras [18] used the C-space method to determine the interference at the cutter contact point. When global interference exists, the cutter axis in the C-space was rotated to obtain a new cutter position without interference. Jun et al. proposed a C-space approach to find the optimal tool orientation by considering the local gouging-free and global tool collision-free in five-axis machining [19].

This study proposes a new method for global interference detection of five-axis machining of complex surfaces. The boundary of the initial detection area is established through intersection operation of the part surface and four extreme planes. Then, the validity of the detection points in the detection area is screened by the four-sided constraint method, and the most serious interference point is found through the subdivision technology. The details of global interference detection and elimination are described in the subsequent sections.

2 Defining coordinate systems and the cutter surface

2.1 Establishing the coordinate systems

In order to conduct interference detection, three coordinate systems should be established first. As shown in Fig. 2, the

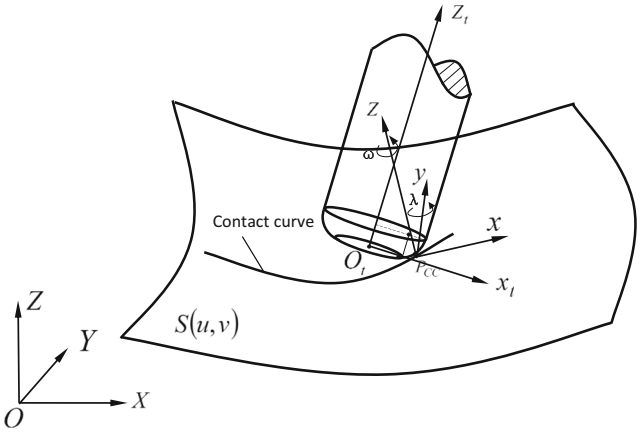

Fig. 2 Three-coordinate systems

part surface is expressed as S (u (t), v (t)), and X, Y, and Z represent the three axes of the part coordinate system; the coordinate origin O is located at the lower left corner of the part. A local coordinate system (x, y, z) is a dynamic coordinate system whose origin is located at each cutter contact (CC) point. The x-axis direction is the feed tangent direction of the CC point; the z-axis direction is the normal direction of the CC point; and the y-axis direction is determined based on the right-hand rule. The cutter coordinate system is represented as x_t, y_t, and z_t, and its coordinate origins O_t are located at the center of the bottom surface of the tool, where z_t coincides with the cutter axis direction. The angles λ and ω represent the angles at which the cutter rotates about the y-axis and the z-axis, respectively. The angles λ and ω are also known as the rear angle and the tilt angle of the cutting tool, respectively.

2.2 The cutter surface model

The fillet-end milling cutter consists of the following three parts: cylindrical surface, toroidal surface, and cutter bottom plane. The model and parameters of the cutter are shown in Fig. 3.

As shown in Fig. 3, the bottom radius of the fillet-end cutter is R_1, the tool radius at the torus is R_2, and φ is the rotation angle of the cutter from $+x_t$. H is the distance from any point on the cylinder surface to the lower end of the tool cylinder, and θ is the corresponding toroidal angle at any point on the torus. According to the geometric characteristics of the fillet-end cutter, cylindrical surface T_L, circular surface T_S, and cutter bottom plane T_U in the tool coordinate system can be given as in Eq. (1):

$$\begin{aligned} \mathrm{T}(\theta,\varphi) &= T_U(\theta,\varphi)\cup T_S(\theta,\varphi)\cup T_L(\theta,\varphi) \\ &= \begin{bmatrix} x_t \\ y_t \\ z_t \end{bmatrix} = \begin{bmatrix} R_1 cos\varphi \\ R_1 sin\varphi \\ 0 \end{bmatrix} \cup \begin{bmatrix} (R_1 + R_2 sin\theta) cos\varphi \\ (R_1 + R_2 sin\theta) sin\varphi \\ R_2(1-cos\theta) \end{bmatrix} \cup \begin{bmatrix} (R_1 + R_2) cos\varphi \\ (R_1 + R_2) sin\varphi \\ R_2 + H \end{bmatrix} \end{aligned} \tag{1}$$

2.3 Calculation of the cutter location point

When the radius of the cutter, the coordinate value of the CC point, and the rear and tilt angles of the tool axis are known, the coordinates of the cutter location point can be obtained at any CC point through the coordinate transformation matrix. In this paper, the cutter location (CL) point is the origin of the cutter coordinate system, which is located at the center of the lower end face of the fillet-end cutter. The coordinate of the CL point in the part coordinate system can be obtained by two coordinate transformations, and its final expression is shown as follows [20]:

$$\begin{bmatrix} X_{cLi} \\ Y_{cLi} \\ Z_{cLi} \\ 1 \end{bmatrix} = \begin{bmatrix} -f_x(R_1\cos\lambda + R_2\sin\lambda)\cos\omega - b_x(R_1\cos\lambda + R_2\sin\lambda)sin\omega + n_x[R_1 sin\lambda + R_2(1-cos\lambda)] + X_{CC_i} \\ -f_y(R_1\cos\lambda + R_2\sin\lambda)\cos\omega - b_y(R_1\cos\lambda + R_2\sin\lambda)sin\omega + n_y[R_1 sin\lambda + R_2(1-cos\lambda)] + Y_{CC_i} \\ -f_z(R_1\cos\lambda + R_2\sin\lambda)\cos\omega - b_z(R_1\cos\lambda + R_2\sin\lambda)sin\omega + n_z[R_1 sin\lambda + R_2(1-cos\lambda)] + Z_{CC_i} \\ 1 \end{bmatrix} \tag{2}$$

In the above-mentioned formula, $(f_x,\ f_y,\ f_z) = {}^{S_t}/_{|S_t|}$ represents the direction cosine of the tangential vector along the tool path direction at the CC point. $(n_x,\ n_y,\ n_z) = \frac{S_u \times S_v}{|S_u \times S_v|} = n$ represents the direction cosine of the normal vector at the CC point. $(b_x,\ b_y,\ b_z) = \frac{n \times S_t}{|n \times S_t|}$ represents the direction cosine of the y-axis in the part coordinate system, and $(X_{CC_i},\ Y_{CC_i},\ Z_{CC_i})$ represents the coordinate value of the CC point in the part coordinate system.

2.4 Conversion matrix from tool coordinate system to part coordinate system

Supposing the angles B and C represent the rotation angle of the cutter around the Y-axis and the Z-axis, respectively, when the tool axis vector z_t is (0, 0, 1, 0), the direction cosines of the vector z_t in the part coordinate system are as follows:

$$\begin{aligned} Z_T &= [0\ 0\ 1\ 0]\cdot \mathrm{Rot}(Y,\theta_B)\cdot \mathrm{Rot}(Z,\theta_C) \\ &= \begin{bmatrix} 0 \\ 0 \\ 1 \\ 0 \end{bmatrix}^T \begin{bmatrix} \cos B & 0 & -\sin B & 0 \\ 0 & 1 & 0 & 0 \\ \sin B & 0 & \cos B & 0 \\ 0 & 0 & 0 & 1 \end{bmatrix} \begin{bmatrix} cosC & sinC & 0 & 0 \\ -sinC & cosC & 0 & 0 \\ 0 & 0 & 1 & 0 \\ 0 & 0 & 0 & 1 \end{bmatrix} \\ &= [sinBcosC\ \ sinBsinC\ \ cosB\ 0] \end{aligned} \tag{3}$$

$$\text{Set } a = \sin B\cos C,\ b = \sin B\sin C,\ c = \cos B \tag{4}$$

The direction cosine Z_T in the workpiece coordinate system is:

$$Z_T = \left\{ \frac{a}{\sqrt{a^2+b^2+c^2}}, \frac{b}{\sqrt{a^2+b^2+c^2}}, \frac{c}{\sqrt{a^2+b^2+c^2}} \right\} = \{ a \quad b \quad c \} \tag{5}$$

The axis y_t of the cutter coordinate system is defined in the part coordinate system as:

$$Y_T = \frac{Z_T \times V_F}{|Z_T \times V_F|} \tag{6}$$

In the above-mentioned equation, V_F represents the direction vector of the current cutter movement. Assuming that the current CC point is $(X_{cci}, Y_{cci}, Z_{cci})$, the next CC point is $(X_{cc(i+1)}, Y_{cc(i+1)}, Z_{cc(i+1)})$. V_F can, then, be expressed as:

$$V_F = \{ X_{cc(i+1)} - X_{cci}, Y_{cc(i+1)} - Y_{cci}, Z_{cc(i+1)} - Z_{cci} \} \tag{7}$$

$$\text{Set } m = X_{cc(i+1)} - X_{cci},\ n = Y_{cc(i+1)} - Y_{cci} \text{ and } p = Z_{cc(i+1)} - Z_{cci} \tag{8}$$

$$\text{Then, } V_F = \{m, n, p\} \tag{9}$$

Substituting Z_T and V_F into the following equation, the direction cosine of the axis y_t in the workpiece coordinate system can be obtained as follows:

$$Y_T = \frac{Z_T \times V_F}{|Z_T \times V_F|} = \left\{ \frac{b\cdot p - c\cdot n}{|Z_T \times V_F|}, \frac{c\cdot m - a\cdot p}{|Z_T \times V_F|}, \frac{a\cdot n - b\cdot m}{|Z_T \times V_F|} \right\} \tag{10}$$

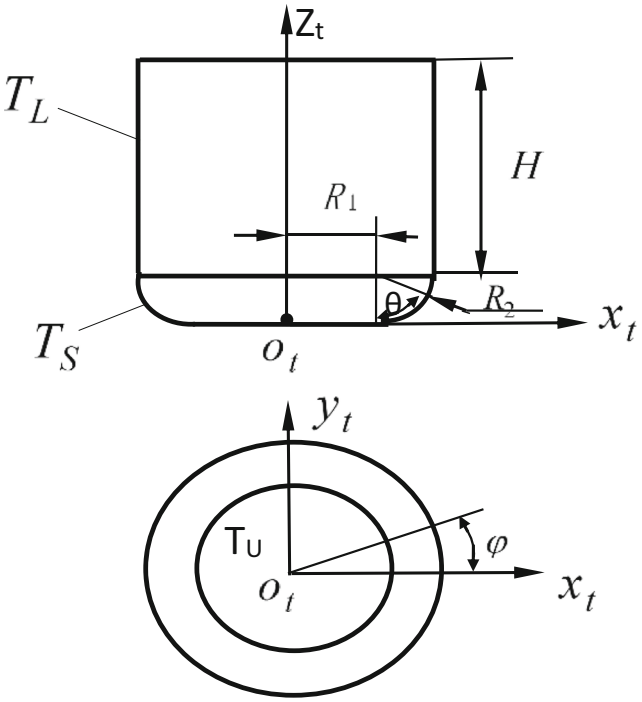

Fig. 3 The model of cutter surface

The direction cosine of the axis x_t in the workpiece coordinate system can be expressed as:

$$X_T = \frac{Y_T \times Z_T}{|Y_T \times Z_T|} = \left\{ \frac{e}{|Y_T \times Z_T|}, \frac{g}{|Y_T \times Z_T|}, \frac{k}{|Y_T \times Z_T|} \right\} \tag{11}$$

In the above-mentioned formula,

$$\begin{aligned} e &= \frac{1}{|Z_T \times V_F|}\{(m{\cdot}c - a{\cdot}p){\cdot}c - (a{\cdot}n - b{\cdot}m){\cdot}b\} \\ g &= \frac{1}{|Z_T \times V_F|}\{(a{\cdot}n - b{\cdot}m){\cdot}a - (b{\cdot}p - c{\cdot}n){\cdot}c\} \\ k &= \frac{1}{|Z_T \times V_F|}\{(b{\cdot}p - c{\cdot}n){\cdot}b - (m{\cdot}c - a{\cdot}p){\cdot}a\} \end{aligned} \tag{12}$$

The conversion matrix from the tool coordinate system to the part coordinate system can be obtained as follows:

$$M_1 = \begin{bmatrix} a_{11} & a_{12} & a_{13} & X_{cLi} \\ a_{21} & a_{22} & a_{23} & Y_{cLi} \\ a_{31} & a_{32} & a_{33} & Z_{cLi} \\ 0 & 0 & 0 & 1 \end{bmatrix} \tag{13}$$

The elements in the above-mentioned matrix are:

$$(a_{11} \quad a_{21} \quad a_{31}) = X_T \tag{14}$$

$$(a_{12} \quad a_{22} \quad a_{32}) = Y_T \tag{15}$$

$$(a_{13} \quad a_{23} \quad a_{33}) = Z_T \tag{16}$$

The calculations of X_T, Y_T and Z_T in the above-mentioned formula are detailed in Eqs. (5)–(12).

3 Global interference detection

3.1 Generation of the initial detection area

Global interference refers to the interference between the cylindrical surface of a fillet-end milling cutter and the workpiece surface. To improve detection efficiency, this paper develops an efficient and novel method to establish an initial detection area. The process of generating the initial detection area is shown as follows.

Supposing there are two planes F_1 and F_2 that pass through the upper and lower ends of the cutter cylindrical respectively, as shown in Fig. 4. If the coordinate value of the center point O_u on the upper end in the cutter coordinate system is (0, 0, h), then, the h represents the length of the cutter. The coordinate value of point O_u in the part coordinate system can be calculated by substituting coordinate transformation matrix M_1 in the following equation.

$$O_u = \begin{bmatrix} X_{O_u} \\ Y_{O_u} \\ Z_{O_u} \\ 1 \end{bmatrix} = M_1 \cdot \begin{bmatrix} 0 \\ 0 \\ h \\ 1 \end{bmatrix} = \begin{bmatrix} ah + X_{cLi} \\ bh + Y_{cLi} \\ ch + Z_{cLi} \\ 1 \end{bmatrix} \tag{17}$$

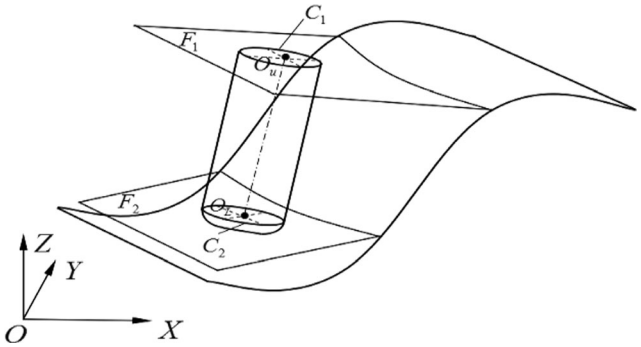

Fig. 4 Generation of two extreme points in the direction X

According to Eq. (5), the coordinate component of the cutter axis vector in the part coordinate system is as follows:

$$Z_T = [a \quad b \quad c]^T = [\text{sinBcosC} \quad \text{sinBsinC} \quad \text{cosB}]^T \tag{18}$$

Supposing the point P is any point on plane F_1 (X, Y, Z), the plane F_1 can, then, be derived from the following equation:

$$Z_T \cdot PO_u = 0 \tag{19}$$

Substituting Eqs. (17) and (18) into the previous equation's results in the equation for plane F_1.

$$aX + bY + cZ - h - aX_{cLi} - bY_{cLi} - cZ_{cLi} = 0 \tag{20}$$

The coordinate value of the center point O_L on the lower end of the cutter cylinder is (0, 0, R_2), and the coordinate values of the point O_L in the workpiece coordinate system can be determined by the conversion matrix M_1.

$$O_L = \begin{bmatrix} X_{O_L} \\ Y_{O_L} \\ Z_{O_L} \\ 1 \end{bmatrix} = M_1 \cdot \begin{bmatrix} 0 \\ 0 \\ R_2 \\ 1 \end{bmatrix} = \begin{bmatrix} aR_2 + X_{cLi} \\ bR_2 + Y_{cLi} \\ cR_2 + Z_{cLi} \\ 1 \end{bmatrix} \tag{21}$$

The equation for plane F_2 is

$$a(X - X_{O_L}) + b(Y - Y_{O_L}) + c(Z - Z_{O_L}) = 0 \tag{22}$$

Substituting Eq. (21) into Eq. (22) results in the equation for plane F_2.

$$aX + bY + cZ - R_2 - aX_{cLi} - bY_{cLi} - cZ_{cLi} = 0 \tag{23}$$

To generate boundaries E_1 and E_2 of the initial detection area, planes F_1 and F_2 need to be intersected with the part surface. Given that the intersection between the curved surface and the plane is more complex, a discrete method is used to carry out the intersection operation. The curved surface is discretised into different stripes of parameter curves. Thus, the intersection of the plane with the surface is converted into the intersection of the plane with the spatial parameter curve. Suppose the surface is discretized along the direction of parameter v, then, the formulas for calculating the intersection of

planes F_1 and F_2 with parametric curve $S(u, v_i)$ are expressed respectively as follows:

$$\begin{cases} \mathrm{aX} + \mathrm{bY} + \mathrm{cZ} - \mathrm{h} - a\mathrm{X}_{\mathrm{cLi}} - b\mathrm{Y}_{\mathrm{cLi}} - c\mathrm{Z}_{\mathrm{cLi}} = 0 \\ X = S_X(u, v_i) \\ Y = S_Y(u, v_i) \\ Z = S_Z(u, v_i) \end{cases} \tag{24}$$

$$\begin{cases} \mathrm{aX} + \mathrm{bY} + \mathrm{cZ} - R_2 - a\mathrm{X}_{\mathrm{cLi}} - b\mathrm{Y}_{\mathrm{cLi}} - c\mathrm{Z}_{\mathrm{cLi}} = 0 \\ X = S_X(u, v_i) \\ Y = S_Y(u, v_i) \\ Z = S_Z(u, v_i) \end{cases} \tag{25}$$

X, Y, and Z in the above-mentioned equations are substituted, respectively, into the first equation of Eqs. (24) and (25). Then, the first equation becomes an equation that contains only one parameter u because v_i has a constant value for each parametric curve. When the value of parameter u is solved by the first equation, the X coordinate value of the intersection point can be obtained by substituting parameters u and v_i into the equation of the curved surface.

Assuming that the variation range of the parameter v of the part surface is $[v_1, v_2]$, given a small increment Δv, then $v_i = v_1 + i\Delta v$ ($i = 0, 1, \ldots, \frac{v_2 - v_1}{\Delta v}$). All the X_i ($i = 0, 1, \ldots, \frac{v_2 - v_1}{\Delta v}$) corresponding to v_i are solved in sequence according to Eq. (24). The maximum value $X_{\max}$ is recorded when the cutter inclination angle $\lambda \geq 0$; otherwise, the minimum value $X_{\min}$ is recorded when $\lambda < 0$.

Similarly, the X_i values of Eq. (25) are solved, in turn, based on the given v_i until $v_i = v_2$. The calculated minimum value, $X_{\min}$, is recorded when the cutter inclination angle $\lambda \geq 0$; otherwise, the maximum value, $X_{\max}$, is recorded when $\lambda < 0$.

According to the following steps, boundary curves E_1 and E_2 of the initial detection area can be generated. In the part coordinate system, the plane π_1: $X = X_{\min}$ is intersected with the part surface to form an intersecting curve, and this intersection curve is named as boundary line E_1. Similarly, the plane π_2: $X = X_{\max}$ is intersected with the machining surface, and the resulting intersection curve is boundary line E_2, as shown in Fig. 5.

The special situation must be considered here. When Eq. (24) is unsolved, this means that there is no intersection between the plane F_1 and the part surface. In this case, the extreme point of X can be found on the boundaries of the part surface. When the cutter inclination angle $\lambda \geq 0$, the maximum value $X_{\max}$ can be obtained from the right boundary of the part surface, and the right boundary is used as the edge E_2 of the initial detection area. Otherwise, when the angle $\lambda < 0$, the minimum value $X_{\min}$ can be obtained from the left boundary of the part surface and the left boundary is used as the edge E_1 of the initial detection area.

The process of generating the boundary lines E_3 and E_4 of the initial detection area is shown as follows:

Firstly, two points with the maximum value $Y_{\max}$ and the minimum value $Y_{\min}$, respectively, should be found from the cylindrical surface of the cutter. These two points generally appear on the circle boundaries of the upper and lower ends of the cutter cylinder. When tilt angle $\omega \geq 0$, the point with the maximum $Y_{\max}$ is located on the circle boundary of the upper end of the cutter cylinder, and the point with the minimum value $Y_{\min}$ is located on the circle boundary of the lower end of the cutter cylinder. When $\omega < 0$, the situation is the opposite.

The equations for circle boundary C_1 on the upper end and circle boundary C_2 on the lower end of the cutter cylinder, as shown in Fig. 4, can be obtained in the part coordinate system by the following:

$$C_1 = \begin{bmatrix} \mathrm{X_{C1}} \\ \mathrm{Y_{C1}} \\ \mathrm{Z_{C1}} \\ 1 \end{bmatrix} = \mathrm{M_1} \cdot \begin{bmatrix} (\mathrm{R_1} + \mathrm{R_2})\cos\varphi \\ (\mathrm{R_1} + \mathrm{R_2})\sin\varphi \\ \mathrm{R_2} + \mathrm{H} \\ 1 \end{bmatrix} \tag{26}$$

$$C_2 = \begin{bmatrix} \mathrm{X_{C2}} \\ \mathrm{Y_{C2}} \\ \mathrm{Z_{C2}} \\ 1 \end{bmatrix} = \mathrm{M_1} \cdot \begin{bmatrix} (\mathrm{R_1} + \mathrm{R_2})\cos\varphi \\ (\mathrm{R_1} + \mathrm{R_2})\sin\varphi \\ \mathrm{R_2} \\ 1 \end{bmatrix} \tag{27}$$

When $\omega \geq 0$, substituting Eq. (13) into Eqs. (26) and (27), respectively, and seeking the extreme value for Y, the point $\mathrm{P_T}$ with the maximum value $Y_{\max}$ on circle boundary C_1 and the point $\mathrm{P_L}$ with the minimum value $Y_{\min}$ on the circle boundary C_2 can be obtained, and the coordinate values of points $\mathrm{P_T}$ and $\mathrm{P_L}$ are given in the following:

$$\mathrm{P_T} = \begin{bmatrix} \mathrm{X_{P_T}} \\ \mathrm{Y_{max}} \\ \mathrm{Z_{P_T}} \end{bmatrix} = \begin{bmatrix} a_{11}(R_1 + R_2)\cos\vartheta_1 + a_{12}(R_1 + R_2)\sin\vartheta_1 + a_{13}h + \mathrm{X_{cLi}} \\ a_{21}(R_1 + R_2)\cos\vartheta_1 + a_{22}(R_1 + R_2)\sin\vartheta_1 + a_{23}h + \mathrm{Y_{cLi}} \\ a_{31}(R_1 + R_2)\cos\vartheta_1 + a_{32}(R_1 + R_2)\sin\vartheta_1 + a_{33}h + \mathrm{Z_{cLi}} \end{bmatrix} \tag{28}$$

$$\mathrm{P_L} = \begin{bmatrix} \mathrm{X_{P_L}} \\ \mathrm{Y_{min}} \\ \mathrm{Z_{P_L}} \end{bmatrix} = \begin{bmatrix} a_{11}(R_1 + R_2)\cos\vartheta_2 + a_{12}(R_1 + R_2)\sin\vartheta_2 + a_{13}R_2 + \mathrm{X_{cLi}} \\ a_{21}(R_1 + R_2)\cos\vartheta_2 + a_{22}(R_1 + R_2)\sin\vartheta_2 + a_{23}R_2 + \mathrm{Y_{cLi}} \\ a_{31}(R_1 + R_2)\cos\vartheta_2 + a_{32}(R_1 + R_2)\sin\vartheta_2 + a_{33}R_2 + \mathrm{Z_{cLi}} \end{bmatrix} \tag{29}$$

In the above-mentioned formula, $\vartheta_1 = tan^{-1}\left(\frac{a_{22}}{a_{21}}\right)$, $\vartheta_2 = tan^{-1}\left(\frac{a_{22}}{a_{21}}\right) - \pi$.

The plane π_3 is defined as: $Y = Y_{\min}$, and it is intersected with the machined surface, and the resulting intersection curve is the boundary line E_3 of the detection area. Similarly, the plane π_4 is defined as $Y = Y_{\max}$ and is intersected with the machined surface, and the resulting intersection curve is boundary line E_4. Thus, the area enclosed by the boundary lines of E_1, E_2, E_3, and E_4 on the machined surface is the initial interference detection region Ω_1, as shown in Fig. 5.

It can be seen from Fig. 5 that the projection of the initial detection region Ω_1 on the XOY plane is a rectangular area Re surrounded by four straight lines L_1 ($X = X_{\min}$), L_2 ($X = X_{\max}$), L_3 ($Y = Y_{\min}$), and L_4 ($Y = Y_{\max}$). To determine whether the cutter cylinder surface interferes with the machined surface, the initial detection area should be discretised to form the

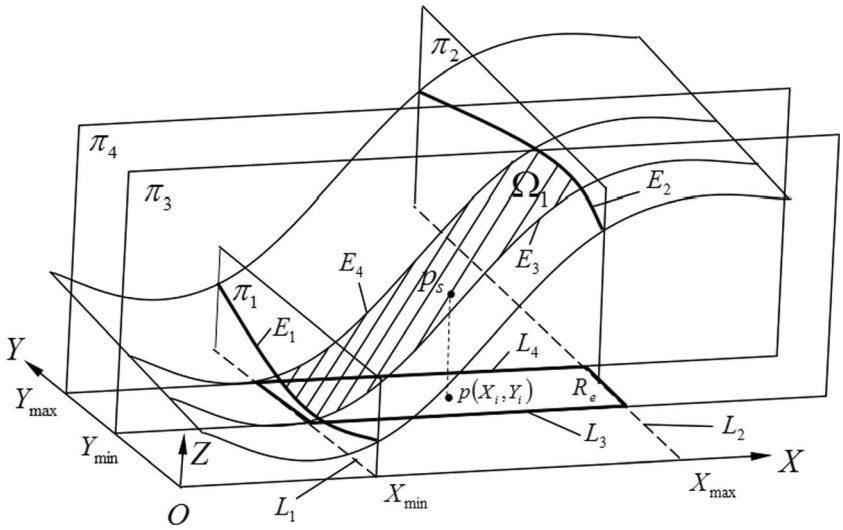

Fig. 5 Generation of the initial detection area

initial detection point set. In order to ensure the uniformity of the discrete points, the dispersion of the detection points is carried out in the projection area *Re* rather than in the domain of parameters *u* and *v* of the part surface. Given a small increment Δx and Δy, rectangle projection area *Re* is uniformly dispersed along the *X* and *Y* axes, respectively, and the coordinates of the discrete point $p_{i,j}$ are $X_i = X_{min} + i\Delta_X (i = 0, 1, \cdots)$ and $Y_i = Y_{min} + j\Delta_Y (j = 0, 1, \cdots)$. Substituting X_i and Y_i into the part surface equations $X = S_X(u, v)$ and $Y = S_Y(u, v)$ to solve for the values of *u* and *v*, if the values of the *u* and *v* can be solved, then there must be a corresponding detection point P_s on the initial detection area Ω_1, as shown in Fig. 5. If the equations $X = S_X(u, v)$ and $Y = S_Y(u, v)$ have no solution, it means that there is no corresponding detection point P_s on the part surface; so, this discrete point is removed and, then, continued to deal with the next discrete point. The *Z* coordinates of detection point P_s can be obtained by substituting the values of *u* and *v* into the equation of $Z = S_Z(u, v)$.

3.2 Screening of effective detection points

In the initial detection area Ω_1, there may be some points that are located below or above the two ends of the cylinder body of the cutter. To improve detection efficiency, only points where interference may occur are detected. These points are named as effective detection points. Therefore, all the detection points in the initial detection area Ω_1 need to be effectively screened.

Firstly, planes F_3 and F_4 that are tangent to the cutter cylinder surface are established. Tangent plane F_3 passes through the point with the maximum Y value, and tangent plane F_4 passes through the point with the minimum Y value. Assuming the cutter tilt angle $\omega \geq 0$, the point with the maximum Y value is point P_T, as shown in Fig. 6, which is located on the circle boundary of the upper end of the cutter cylinder. The point with the minimum Y value is point P_L, as shown in Fig. 6, which is located on the circle boundary of the lower end of the cutter cylinder. Here, the normal directions of the four planes, which are the planes F_1, F_2, F_3, and F_4, all point to the inside of the cutter body, and the symbols N_1, N_2, N_3, and N_4 denote the normal vectors of planes F_1, F_2, F_3, and F_4, respectively. Then,

$$N_1 = -Z_T = \{-a, -b, -c\} \tag{30}$$

$$N_2 = Z_T = \{a, b, c\} \tag{31}$$

$$N_3 = \frac{\overrightarrow{P_T O_u}}{\left|\overrightarrow{P_T O_u}\right|} \tag{32}$$

$$N_4 = \frac{\overrightarrow{P_L O_L}}{\left|\overrightarrow{P_L O_L}\right|} \tag{33}$$

Assuming that the point P (X_P, Y_P, Z_P) is any detection point in the initial detection area Ω_1, the following inequality can be used to determine whether the point P is an effective detection point.

$$\begin{cases} N_1 \cdot (P - O_u) \geq 0 \\ N_2 \cdot (P - O_L) \geq 0 \\ N_3 \cdot (P - P_T) \geq 0 \\ N_4 \cdot (P - P_L) \geq 0 \end{cases} \tag{34}$$

In the above-mentioned equations, the coordinate values of points O_u, O_L, P_T, and P_L can be calculated by Eqs. (17), (21), (28), and (29), respectively.

All of the initial detection points satisfying inequality (34) form an effective detection area V_a, as shown in Fig. 6.

3.3 Interference detection

For each effective detection point in the area V_a as shown in Fig. 6, the distance between the valid detection point and the

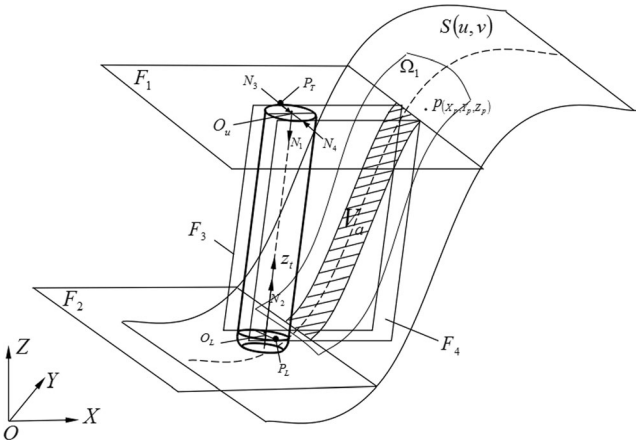

Fig. 6 Generation of valid detection area

cutter axis is used to judge whether there is interference between the cutter cylinder surface and the part surface. The equation expression of the line that passes through the cutter location point and the cutter axis can be given as follows:

$$\frac{X-X_{cLi}}{a}=\frac{Y-Y_{cLi}}{b}=\frac{Z-Z_{cLi}}{c} \tag{35}$$

The distance between the valid detection point P_s and the cutter axis can be obtained by the following equation:

$$d=\sqrt{(X_{P_s}-X_{cLi}-at)^2+(Y_{P_s}-Y_{cLi}-bt)^2+(Z_{P_s}-Z_{cLi}-ct)^2} \tag{36}$$

where,

$$t=a(X_{P_s}-X_{cLi})+b(Y_{P_s}-Y_{cLi})+c(Z_{P_s}-Z_{cLi})$$

Given the coordinate values of point P_s and substituting Eqs. (2) and (5) into Eq. (36), the distance from point P_s to the cutter axis can be obtained.

According to Eq. (36), the distances of all valid detection points in area V_a are sequentially calculated, and the detection point P^1_{min} that corresponds to minimum distance d^1_{min} is recorded. To improve detection accuracy, a subdivision technique is used to find out whether there is the shortest distance between the cutter axis and the effective detection area V_a on the part surface. The detailed process is shown in the subsequent discussion:

According to coordinate values X^1 and Y^1 of point P^1_{min}, the projection point P^1_{XY} of the detection point P^1_{min} in the rectangle projection area Re is determined. Using point P^1_{XY} as the center point, a smaller rectangle area R^1_e is established around the center point and its four boundary lines are L^1_1 $(X^1-\Delta X/2)$, L^1_2 $(X^1+\Delta X/2)$, L^1_3 $(Y^1-\Delta Y/2)$, and L^1_4 $(Y^1+\Delta Y/2)$, respectively.

The smaller increments δ_X and δ_Y are given, and the new rectangle area R^1_e is uniformly dispersed along the X and Y axes, respectively. If a new valid detection point P^2_{min} corresponding to the discrete point P^2_{XY} in the rectangle area R^1_e can be found, in other words, the value d^2_{min} of the distance between the detection point P^2_{min} and the cutter axis is less than d^1_{min}, then, point P^1_{min} is replaced with point P^2_{min}. A similar method is used to establish a new smaller rectangle area R^2_e with the point P^2_{XY} as the center and the four boundaries of the rectangle area R^2_e are L^2_1 $(X^2-\Delta X/4)$, L^2_2 $(X^2+\Delta X/4)$, L^2_3 $(Y^2-\Delta Y/4)$, and L^2_4 $(Y^2+\Delta Y/4)$, respectively. X^2 and Y^2 are the coordinate values of the points P^2_{XY} and P^2_{min}. The new rectangle area R^2_e is uniformly dispersed by the small increments $\delta_X/2$ and $\delta_Y/2$. Repeat the above-mentioned steps until the point P^n_{min} with the minimum value d^n_{min} satisfying the accuracy requirement is found.

If any distance between the detection point, which corresponds to the discrete point in the area R^1_e, and the cutter axis is greater than the distance d^1_{min}, given the changed increments $\delta_X/2$ and $\delta_Y/2$, the rectangle area R^1_e is re-dispersed along the X and Y axes until the new minimum distance d^n_{min} is found.

The interference detection can be carried out by the following inequality:

$$d^n_{min}<(R_1+R_2) \tag{37}$$

If the above-mentioned inequality is satisfied, there is interference between the cutter and part surface; otherwise, there will be no interference.

4 Interference elimination

If interference is detected by the above-mentioned method before the tool path planning, the elimination of interference

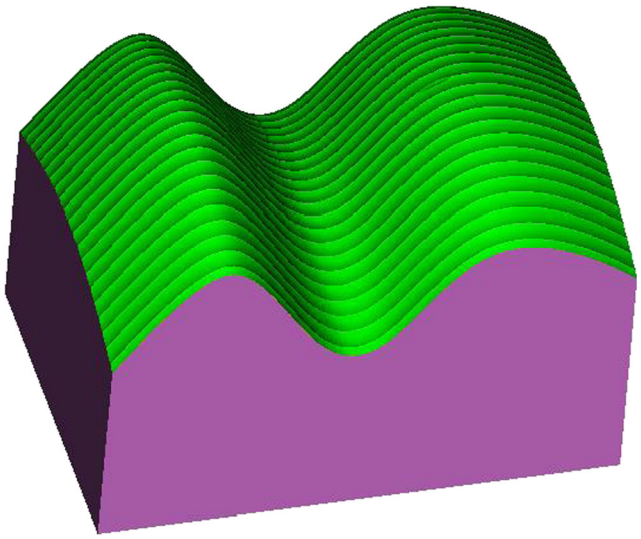

Fig. 7 The surface of the first example part

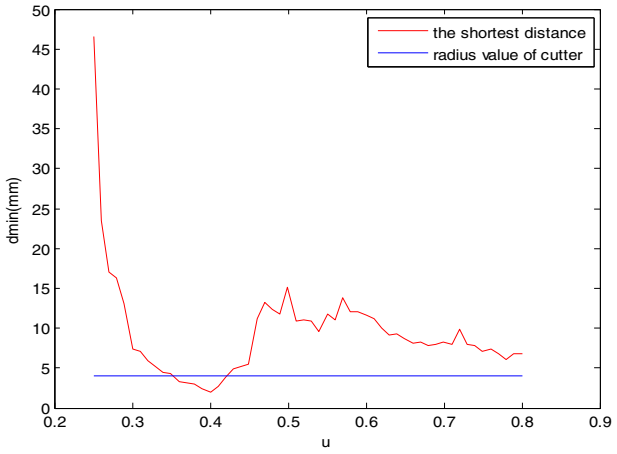

(a) The shortest distance along the curve (u, 0.47)

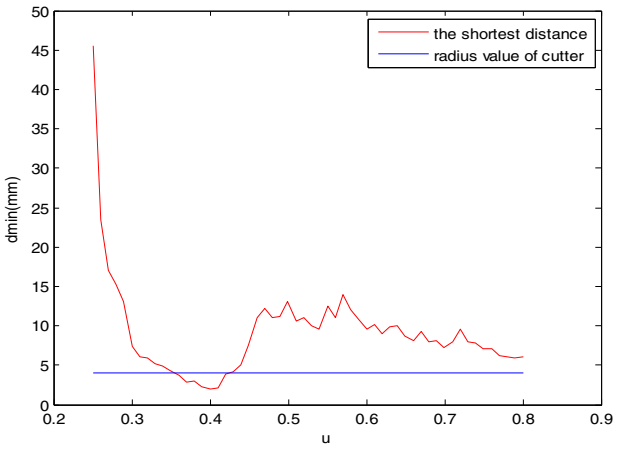

(b) The shortest distance along the curve (u, 0.53)

Fig. 8 The shortest distance for $\lambda_0 = 15^{\circ}$

can be realized by a method of adjusting the inclination angle of the cutter.

Assuming that the interference point with the smallest distance d_{sm} from the cutter axis to the part surface is detected as P_{sm} $(X_{P_{sm}}, \mathrm{Y_{Psm}}, \mathrm{Z_{Psm}})$, to avoid the interference between the cutter surface and part surface, the smallest distance d_{sm} should be greater than $(R_1 + R_2)$. It is assumed that the rear angle of the cutter is λ' without interference and the angle λ' can be calculated by the following inequality:

$$d_{sm} \geq (R_1 + R_2) \tag{38}$$

According to Eq. (36), the above-mentioned inequality can be further written as follows:

$$\sqrt{(X_{P_{sm}} - X_{cLi} - at)^2 + (Y_{P_{sm}} - Y_{cLi} - bt)^2 + (Z_{P_{sm}} - Z_{cLi} - ct)^2} \geq (R_1 + R_2) \tag{39}$$

Where,

$$\mathrm{t} = \mathrm{a}(\mathrm{X}_{P_{sm}} - X_{cLi}) + \mathrm{b}(Y_{P_{sm}} - Y_{cLi}) + c(Z_{P_{sm}} - Z_{cLi})$$

If the tilt angle of the cutter is unchanged, when equal (2) for calculating the coordinate values (X_{cLi}, Y_{cLi}, Z_{cLi}) of CL point is substituted into inequality (39), then, inequality (39) becomes an inequality containing only variable λ'. The boundary value of the rear angle λ' without interference can be obtained by the Newton iterative method.

5 Simulation and experiment

In order to test the validity and the correctness of the algorithm proposed in this paper, two examples are used to verify the algorithm, and the interference detection calculation is realized by using the MATLAB programming software.

5.1 The first example

The first example surface is defined as a cubic NURBS surface with parameters u and v. The coordinates values of 32 control grid points of the example surface are as follows: (0, 0, 60), (22.57, 0, 91.46), (37.30, 0, 98.11), (59.37, 0, 54.5), (78.93, 0, 52.03), (95.86, 0, 82.49), (120, 0, 94.34), (150, 0, 70), (0, 40, 75), (22.57, 40, 106.46), (37.3, 40, 113.10), (59.37, 40, 69.49), (78.93, 40, 62.03), (95.86, 40, 97.49),

Table 1 The interference along the parameter curve S (u, 0.47)

CC point	d_{min}(mm))	Adjusted $\lambda'(^{\circ})$	(X,Y,Z,B,C) of CL point before the adjustment	(X,Y,Z,B,C) of CL point after the adjustment
(0.36, 0.47)	0.69	14.22, 0.04	(53.78, 47.71, 80.21, − 69.08, 179.96)	(53.76, 47.70, 80.18, − 68.30, 179.91)
(0.37, 0.47)	1.41	13.45, 0.07	(54.81, 47.70, 78.74, − 68.03, 179.99)	(54.78, 47.70, 78.67, − 66.49, 179.90)
(0.38, 0.47)	1.79	13.09, 0.11	(55.80, 47.69, 77.35, − 66.70, 179.98)	(55.77, 47.70, 77.26, − 64.70, 179.89)
(0.39, 0.47)	1.80	12.98, 0.12	(56.79, 47.69, 76.03, − 65.00, 179.98)	(56.75, 47.69, 75.93, − 62.99, 179.88)
(0.40, 0.47)	1.37	12.63, 0.18	(57.74, 47.68, 74.79, − 62.89, 179.99)	(57.71, 47.69, 74.67, − 60.52, 179.82)
(0.41, 0.47)	0.57	14.16, 0.13	(58.70, 47.69, 73.62, − 60.37, 179.93)	(58.69, 47.69, 73.58, − 59.53, 179.86)

Table 2 The interference along the parameter curve S (u, 0.53)

CC point	d_{min}(mm))	Adjusted $\lambda'(^{\circ})$	(X,Y,Z,B,C) of CL point before the adjustment	(X,Y,Z,B,C) of CL point after the adjustment
(0.36, 0.59)	0.47	14.48, 0.29	(53.78, 58.01, 79.88, − 68.87, 179.81)	(53.77, 58.01, 79.86, − 68.38, 179.71)
(0.37, 0.59)	1.17	13.56, 0.38	(54.81, 58.04, 78.41, − 67.79, 179.93)	(54.78, 58.03, 78.34, − 66.33, 179.62)
(0.38, 0.59)	1.53	13.20, 0.39	(55.81, 58.07, 77.02, − 66.44, 179.98)	(55.78, 58.06, 76.93, − 64.67, 179.61)
(0.39, 0.59)	1.52	13.23, 0.40	(56.80, 58.09, 75.69, − 64.72, 179.99)	(56.77, 58.08, 75.61, − 62.99, 179.60)
(0.40, 0.59)	1.09	13.75, 0.30	(57.76, 58.09, 74.44, − 62.61, 179.89)	(57.74, 58.09, 74.39, − 61.38, 179.60)
(0.41, 0.59)	0.31	14.58, 0.31	(58.71, 58.09, 73.28, − 60.09, 179.68)	(58.71, 58.09, 73.26, − 59.68, 179.58)

(120, 40, 109.3), (150, 40, 85), (0, 60, 75), (22.57, 60, 106.46), (37.3, 60, 113.10), (59.37, 60, 69.49), (78.93, 60, 67.03), (95.86, 60, 97.49), (120, 60, 109.3), (150, 60, 85), (0, 100, 60), (22.57, 100, 91.46), (37.3, 100, 98.11), (59.37, 100, 54.49), (78.93, 100, 52.03), (95.86, 100, 82.49), (120, 100, 94.34), and (150, 100, 70). The node vectors in u and v directions are expressed as $u = \{0, 0, 0, 0, 1/5, 2/5, 3/5, 4/5, 1, 1, 1, 1\}$ and $v = \{0, 0, 0, 0, 1, 1, 1, 1\}$. All of the weight factors corresponding to control grid points are set to 1. The example surface is shown as in Fig. 7.

The sizes of fillet-end milling cutter are selected as $R_1 =$ 2 mm, $R_2 = 2$ mm, and $h = 75$ mm. The initial rear angle of the cutter is $\lambda_0 = 15^{\circ}$, and the tilt angle is $\omega_0 = 0$. A method based on equal parameter increment is used to generate the tool path along the direction of the parameter u, and the degree of detection accuracy is 0.01 mm.

It can be seen from Fig. 7 that the region where the interference most likely to occur on the part surface is located in the area corresponding to parameter $u \in [0.25,0.70]$; so, the calculation of interference detection was mainly carried out in the range of u from 0.25 to 0.80. When the cutter is cutting along the parameter curve S (u, 0.47), according to the interference detection algorithm, the global interference exists when the rear angle equals to 15°. The minimum distance d_{min} between the cutter axis and detection area is calculated at every CC point along the parameter curve S (u, 0.47), as shown in Fig. 8a. It can be seen from Fig. 8a that the interference occurs within the range of parameter u from 0.36 to 0.42 and there are six CC points where the interference occurs. The shortest distances d_{min} corresponding to six CC points are shown in Table 1. Similarly, when the cutting is performed along the parameter curve S (u, 0.53), the interference still takes place within the range of parameter u from 0.36 to 0.42, as shown in Fig. 8b. The shortest distance corresponding to six CC points can be calculated by the interference detection algorithm proposed in this paper, as shown in Table 2.

When the initial rear angle λ_0 is set to 20°, more serious interference took place. For example, when the cutting is along the parameter curve S (u, 0.47), the interference range of parameter u changes from [0.36, 0.42] to [0.30, 0.46], and there are sixteen points at which the interference between tool and workpiece occurs. The shortest distances corresponding to sixteen CC points are all less than 5 mm, as shown in Fig. 9.

In order to verify the correctness of the interference detection method, the cutting simulation of the sample surface was carried out by the VERICUT software, as shown in Fig. 10.

In the process of cutting simulation by VERICUT software, if there is global interference between the tool and the workpiece, in the region where interference occurs, the tool will move along a specially designed path, and the tool does not cut the workpiece during the movement. Cutting continues when the tool crosses the interference region. The specific interference region can be determined from the generated simulation NC program. As shown in Fig. 11, when the rear angle and tilt angle are set to 15° and zero, respectively, a special program block surrounded by green boxes is inserted between the two program segments surrounded by red boxes. This special program block corresponds to the special path of tool movement in the interference region mentioned previously. In other words, it can be seen from Fig. 11a that the global interference between the cutter and the workpiece occurs between

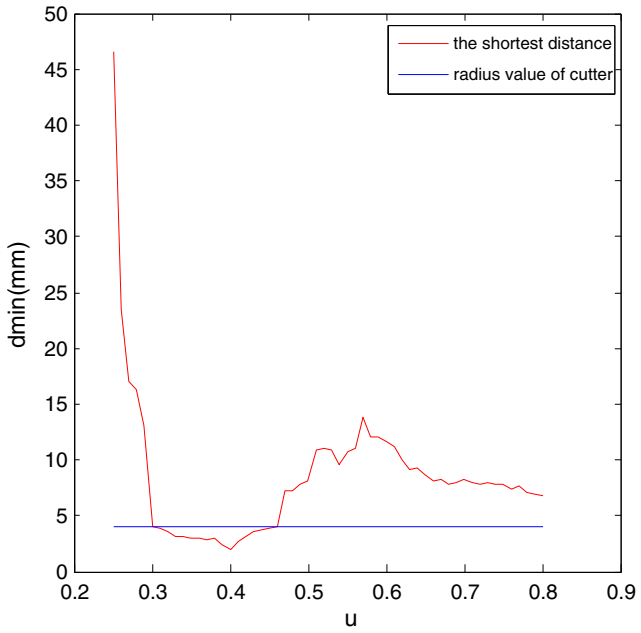

Fig. 9 The shortest distance for $\lambda_0 = 20^{\circ}$

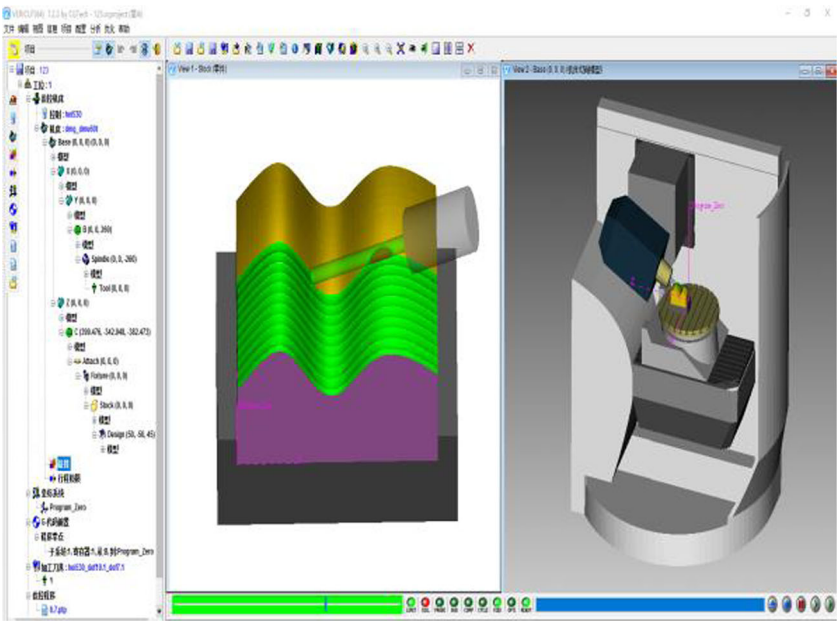

Fig. 10 Cutting simulation by VERICUT software

CL point 1 (53.029, 49.446, 78.463) and point 2 (59.261, 49.447, 70.128). In order to describe more vividly the CL points where interference occurs in the process of tool movement, the CC point corresponding to the CL point on the cutter contact curve can be used to represent the position where interference occurs, as shown in Fig. 11b. The red

```
L X40.65 Y49.446 Z95.393 B-64.485 C180.496
L X41.532 Z94.425 B-65.819 C180.477
L X43.11 Z92.549 B-67.751 C180.45
L X44.665 Z90.55 B-69.155 C180.432
L X46.123 Z88.562 B-70.078 C180.419
L X47.563 Z86.519 B-70.645 C180.412
L X48.965 Z84.475 B-70.883 C180.409
L X50.348 Z82.428 B-70.807 C180.41
L X51.743 Z80.358 B-70.398 C180.415
L X52.431 Z79.34 B-70.06 C180.42
L X52.773 Z78.837 B-69.855 C180.422
L X52.944 Z78.587 B-69.744 C180.424
L X53.029 Z78.463 B-69.686
L X105.249 Y49.833 Z97.783 B-69.678 C180.425
L X105.555 Y49.835 Z97.884 B-69.671
L X105.957 Y49.838 Z98.01 B-69.656
L X106.503 Y49.842 Z98.166 B-69.626
L X107.878 Y49.853 Z98.49 B-69.494 C180.427
L X108.767 Y49.86 Z98.647 B-69.354 C180.429
L X110.006 Y49.87 Z98.798 B-69.051 C180.433
L X111.475 Y49.886 Z98.871 B-68.348 C180.442
L X112.167 Y49.897 Z98.849 B-67.505 C180.454
L X112.27 Y49.906 Z98.804 B-66.504 C180.467
L X111.713 Y49.913 Z98.734 B-65.162 C180.486
L X110.355 Y49.916 Z98.587 B-63.557 C180.509
L X109.302 Z98.433 B-62.644 C180.522
L X108.022 Y49.913 Z98.184 B-61.684 C180.537
L X106.464 Y49.908 Z97.782 B-60.688 C180.552
L X104.389 Y49.897 Z97.067 B-59.655 C180.568
L X102.436 Y49.883 Z96.191 B-59.021 C180.578
L X101.561 Y49.876 Z95.733 B-58.86 C180.58
L X101.208 Y49.872 Z95.537 B-58.82 C180.581
L X59.261 Y49.447 Z70.128 B-58.78
L X59.288 Z70.097 B-58.699 C180.583
L X59.397 Z69.974 B-58.373 C180.588
L X59.83 Z69.497 B-57.032 C180.61
L X60.688 Z68.599 B-54.17 C180.659
```

(a) Partial NC program of cutting simulation

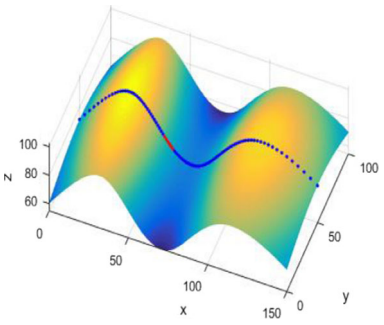

(b) CC points where interference occurs

Fig. 11 Results of cutting simulation along the cutter contact curve $S(u, 0.47)$ for $\lambda_0 = 15^\circ$

Fig. 12 Results of cutting simulation along the cutter contact curve $S(u, 0.47)$ for $\lambda_0 = 20^\circ$

```
L X49.43 Z84.179 B-75.893
L X49.473 Z84.115
L X49.495 Z84.083
L X107.321 Y49.838 Z98.614
L X108.295 Y49.845 Z98.823
L X109.828 Y49.854 Z99.061 B-75.891
L X111.533 Y49.865 Z99.198 B-75.884
L X113.746 Y49.878 Z99.19 B-75.856 C180.388
L X115.367 Y49.887 Z99.059 B-75.807
L X117.847 Y49.902 Z98.671 B-75.646 C180.39
L X119.676 Y49.913 Z98.244 B-75.398 C180.393
L X122.104 Y49.931 Z97.497 B-74.626 C180.402
L X123.289 Y49.948 Z97.022 B-73.348 C180.417
L X123.382 Y49.955 Z96.945 B-72.505 C180.428
L X123.129 Y49.963 Z96.984 B-71.504 C180.44
L X121.143 Y49.977 Z97.489 B-68.557 C180.476
L X119.345 Y49.982 Z97.893 B-66.684 C180.5
L X117.197 Y49.984 Z98.258 B-64.655 C180.527
L X115.735 Z98.425 B-63.372 C180.545
L X114.112 Y49.982 Z98.527 B-62.032 C180.563
L X112.291 Y49.979 Z98.528 B-60.632 C180.583
L X110.213 Y49.972 Z98.371 B-59.17 C180.605
L X109.045 Y49.967 Z98.203 B-58.414 C180.616
L X107.757 Y49.96 Z97.948 B-57.643 C180.628
L X106.303 Y49.952 Z97.566 B-56.855 C180.64
L X104.582 Y49.94 Z96.979 B-56.049 C180.653
L X103.548 Y49.932 Z96.552 B-55.64 C180.66
L X102.284 Y49.921 Z95.952 B-55.227 C180.666
L X100.372 Y49.902 Z94.876 B-54.81 C180.673
L X99.343 Y49.891 Z94.211 B-54.704 C180.675
L X61.921 Y49.45 Z67.697 B-54.652 C180.676
L X61.934 Z67.685 B-54.599 C180.677
L X61.985 Z67.638 B-54.388 C180.68
L X62.396 Z67.273 B-52.656 C180.709
L X62.891 Z66.854 B-50.461 C180.749
```

(a) Part of the generated simulation NC code

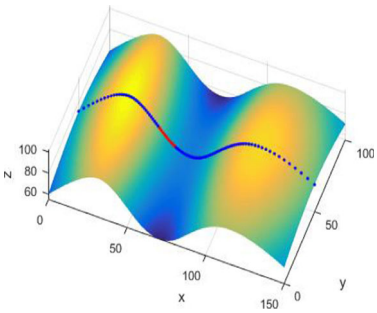

(b) CC points where interference occurs

section of the cutter contact curve indicates that the global interference occurs when the cutter moves in this section, and the blue section indicates that there is no global interference. According to the coordinate values of CL point 1 and CL point 2 in Fig. 11a, the range of parameter u corresponding to interference occurrence can be calculated out. As shown in Fig. 11, when the cutter cuts along the cutter contact curve $S(u, 0.47)$, the range of parameter u corresponding to interference occurrence is from 0.3602 to 0.4199.

Similarly, when the rear angle is set to 20° and the cutter moves along the same cutter contact curve $S(u, 0.47)$, according to the results of cutting simulation shown in Fig. 12, the

Fig. 13 Comparisons between calculated results and VERICUT simulation results

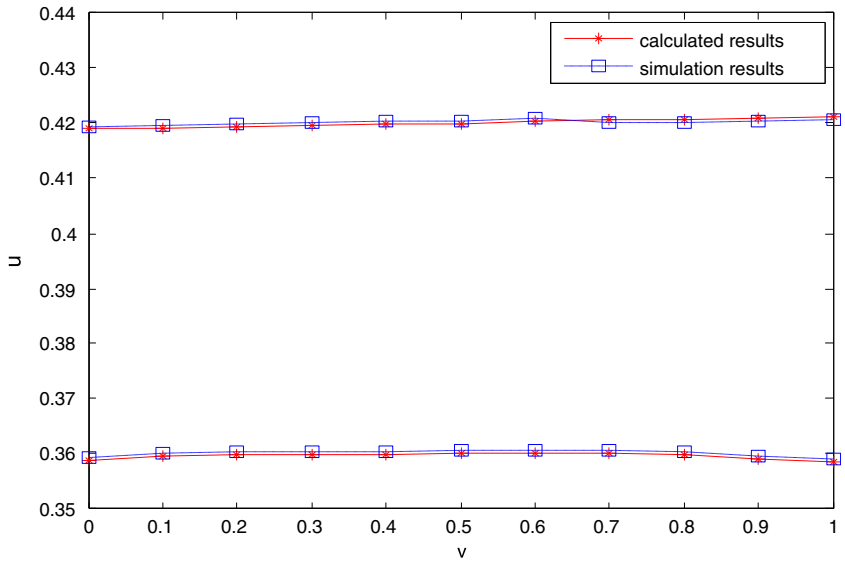

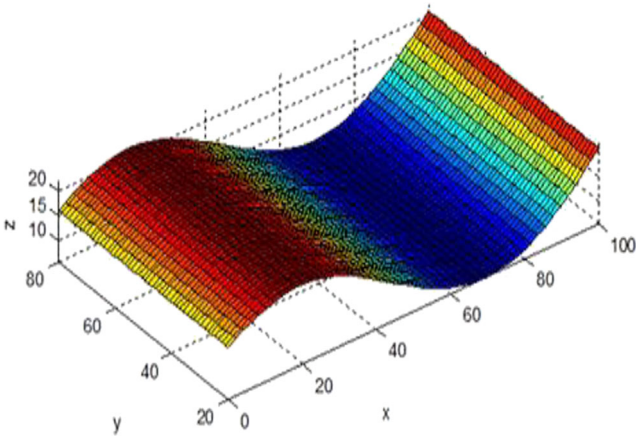

Fig. 14 The second example surface

range of parameter u corresponding to interference occurrence can be calculated, and the result is from 0.299 to 0.4603.

In order to compare the simulation of results VERICUT with the results calculated by the interference detection algorithm, eleven cutter contact curves are used for experimental verification. Each cutter contact curve can be expressed as $S_i(u, i \cdot \Delta v)(i = 0, 1, 2 \cdots 10; \Delta v = 0.1)$. The results of simulation and calculation are shown in Fig. 13. Two red curves obtained by the interference detection algorithm represent the range boundaries of parameter u corresponding to interference occurrence, respectively. Two blue curves obtained by VERICUT simulation indicate the range boundaries of parameter u corresponding to interference occurrence. It can be seen from Fig. 13 that the simulation results and the calculation results are in good agreement.

5.2 The second example

The second example is a free-form surface which is 100 × 60 mm^2 in size and 15 mm in height, as shown in Fig. 14. As can be seen from Fig. 14, the left half of the surface is convex and the right half is concave. When the tool moves from left to right along the parametric curve, the global tool interference mainly occurs on the concave surface corresponding to the parameter u ∈ [0.5,1.0]. A fillet-end milling cutter with a length of 75 mm and a diameter of 10 mm was used for interference simulation and machining the example surface.

Assuming that the tilt angle of the tool is set to 0° during simulation and machining and the degree of detection accuracy is 0.01 mm, according to the interference detection

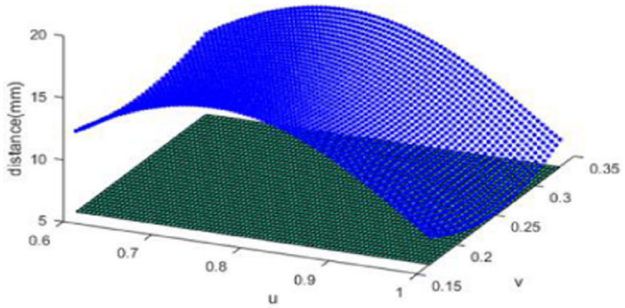

(a) $\lambda_0 = 53.2^\circ$

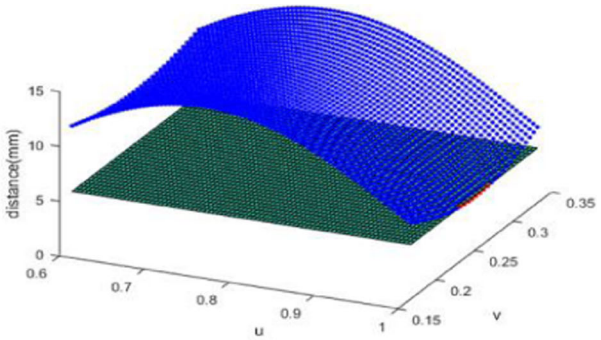

(b) $\lambda_0 = 53.5^\circ$

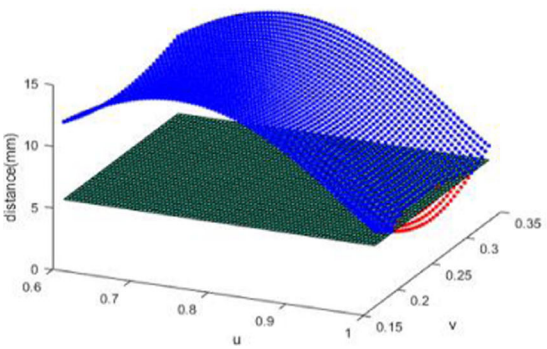

(c) $\lambda_0 = 54.5^\circ$

Fig. 15 Distances between the tool axis and detection points at CC point S ($u = 0.55$, $v = 0.25$)

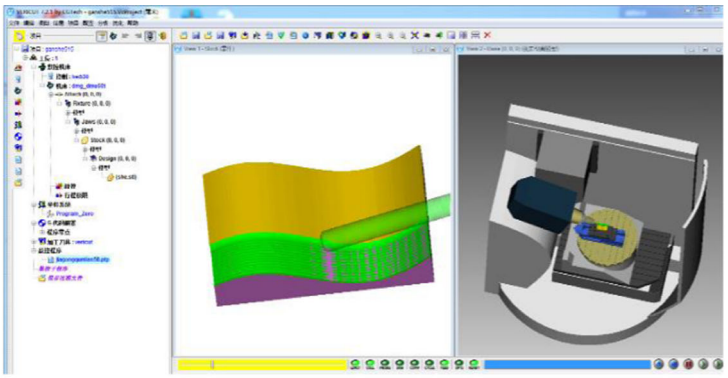

(a) $\lambda_0 = 53.2^\circ$

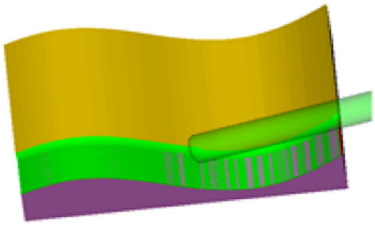

(b) $\lambda_0 = 53.5^\circ$

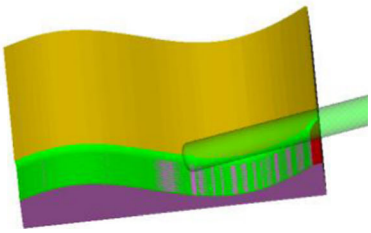

(c) $\lambda_0 = 54.5^\circ$

Fig. 16 Interference simulation at different tool rear angles by the VERICUT software

algorithm proposed in this paper, it can be calculated that there will be no interference collision between the tool and the workpiece when the rear angle of the tool changes from to − 77.25 to 53.22°. When the tool rear angle is set to 53.2, 53.5, and 54.5°, respectively, at the CC point ($u = 0.55$, $v = 0.25$), all distances between the tool axis and detection points in the possible interference area can be calculated out, as shown in Fig. 15. The blue and red dots represent the distance between the tool axis and the detection point, and the green plane is a reference plane, and its corresponding distance value is 5 mm. When the value of distance between the tool axis and the detection point is greater than or equal to 5 mm, it is indicated by blue dots; otherwise, it is indicated by red dots. It can be seen from Fig. 15a that all distances are indicated by blue dots, which means that there is no interference between the tool and the workpiece surface. The red dots below the green plane in Fig. 15 indicate that the distance of the red dot is less than 5 mm, which means that there is interference between the tool and the workpiece. With the increase of tool rear angle, interference becomes more and more serious. As shown in Fig. 15, the number of red dots in Fig. 15c is significantly larger than that in Fig. 15b.

In order to verify the correctness of the results calculated by the interference detection algorithm, the cutting simulation

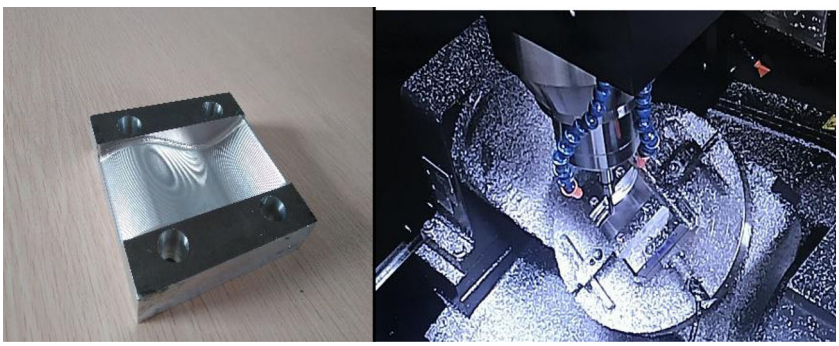

(a) The machined sample surface (b) Machining of example surface

Fig. 17 Physical experiment of the second sample surface

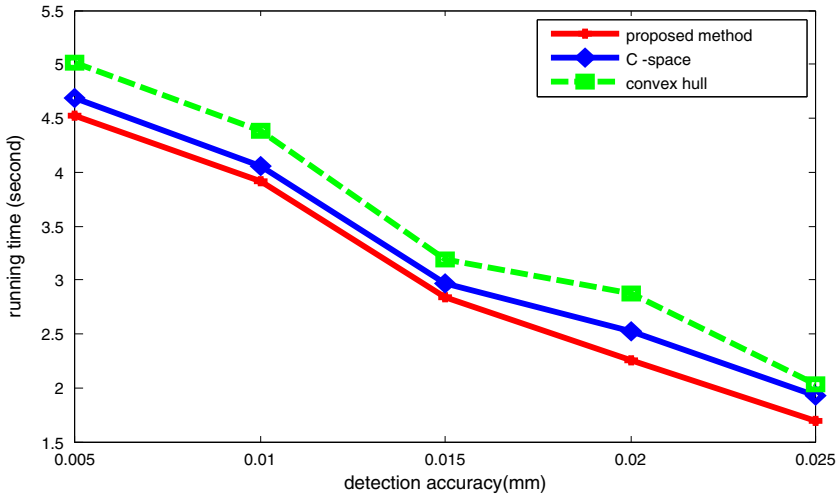

Fig. 18 Comparison of running time of three methods for different detection accuracy

was carried out by using the VERICUT software. Figure 16 shows the simulation results at different tool rear angles. The red regions in Fig. 16 represent the interference area on the part surface. It can be clearly seen that the interference region corresponding to the rear angle of 54.5° is larger than that with the rear angle of 53.5°. Comparing Fig. 15 with Fig. 16, it can be seen that the calculated results are consistent with the simulation results.

The physical experiment of the sample surface was carried out on a five-axis milling machine named JT-GL8-V. The tested surface material is aluminum alloy 7075, and the rear angle of the tool was set to 20°. The machined example surface and the picture of the machining process are shown in Fig. 17a,b.

5.3 Comparison of several different detection methods

In this paper, the detection accuracy is greatly improved by the subdivision technology. For the same detection accuracy, the method proposed in this paper is more efficient than the traditional interference detection methods. To support this conclusion, the proposed algorithm was compared with the traditional convex hull-based method and C-space-based method. Any CC point on the surface of the second sample was used as the experimental point, and the times consumed for interference judgment and elimination by the new method, convex hull-based method, and C-space-based methods were recorded, respectively. For example, when the cutter is located at the CC point (50.35, 10.87), the times consumed for global interference judgment and elimination corresponding to different detection accuracy are shown in Fig. 18. It can be seen from the figure that the new method proposed is more efficient than the two traditional methods and that the higher the detection accuracy, the longer the consuming time.

6 Conclusion

This study presents a novel method for global interference detection of the five-axis machining. A method based on four extreme planes was used to rapidly build the initial interference detection area. The shortest distance between the tool axis and the initial detection area is used to judge whether there is interference collision between the tool and the workpiece. The shortest distance can be obtained by calculating the distance between the discrete point in the detection area and the tool axis. In order to ensure the uniformity of the discrete points, the dispersion of the detection points is carried out in the projection area of the detection region rather than on the part surface. To improve the detection efficiency, the detection points in the initial detection area are screened using the four-sided constraint method, and only the points that meet the screening conditions are selected to form the valid detection area. For improving detection accuracy, subdivision technology is used to achieve high-precision detection. In order to verify the correctness and validity of the algorithm, two examples are used to verify the algorithm. Firstly, interference detection and calculation are carried out by using the MATLAB programming software. Then, the cutting simulation of two example surfaces is carried out on the VERICUT software. By comparing the cutting simulation results with the interference calculation results, it can be seen that they are in good agreement. By comparing the new algorithm with the traditional convex hull- and C-space-based methods, it can be concluded that the new algorithm has higher efficiency. This novel interference detection method proposed in this study can be used in 5-axis end-milling of complex surfaces.

Acknowledgments This research was supported by the National Natural Science Foundation of China under grant no. 51475317. The authors would like to thank the anonymous reviewers for their valuable remarks and comments.

References

1. Chen T, Ye PQ, Wang JS (2005) Local interference detection and avoidance in five-axis NC machining of sculptured surfaces. Int J Adv Manuf Technol 25(3–4):343–349
2. Sun Y, Xu J, Jin C (2016) Smooth tool path generation for 5-axis machining of triangular mesh surface with nonzero genus. Comput Aided Des 79:60–74
3. Dong Z, Yuan J (1993) A formulation for collision identification and distance calculation in motion planning using neural networks. Int J Adv Manuf Technol 8(4):227–234
4. Wu BH, Zhang DH, Luo M, Zhang Y (2013) Collision and interference correction for impeller machining with non-orthogonal four-axis machine tool. Int J Adv Manuf Technol 68(1–4):693–700
5. Ahmed A, Chen ZC (2017) A comprehensive approach to determining minimum cutter lengths for five-axis milling. Int J Adv Manuf Technol 90(5–8):1235–1252
6. Qiao Z, Wang T, Wang Y (2012) Bezier polygons for the linearization of dual NURBS curve in five-axis sculptured surface machining. Int J Mach Tool Manu 53(1):107–117
7. Tang TD, Bohez ELJ (2015) A new collision avoidance strategy and its integration with collision detection for five-axis NC machining. Int J Adv Manuf Technol 81(5–8):1247–1258
8. Lin ZC, Chow JJ (2001) Near optimal measuring sequence planning and collision-free path planning with a dynamic programming method. Int J Adv Manuf Technol 18(1):29–43
9. Wang QH, Li JR, Zhou RR (2006) Graphics-assisted approach to rapid collision detection for multi-axis machining. Int J Adv Manuf Technol 30(9–10):853–863
10. Wang Y, Wang Z, Gindy N (2009) Collision-free machining fixture space design based on parametric tool space for five-axis grinding. Int J Adv Manuf Technol 45(1–2):1–7
11. Lee YS, Chang TC (1995) 2-Phase approach to global tool interference avoidance in 5-axis machining. Comput Aided Des 27(10): 715–729
12. Deng XZ, Li GG, Wei BY, Deng J (2014) Face-milling spiral bevel gear tooth surfaces by application of 5-axis CNC machine tool. Int J Adv Manuf Technol 71(5–8):1049–1057
13. Lin ZW, Shen HG, Gan WF, Fu JZ (2012) Approximate tool posture collision-free area generation for five-axis CNC finishing process using admissible area interpolation. Int J Adv Manuf Technol 62(9–12):1191–1203
14. Tang TD (2014) Algorithms for collision detection and avoidance for five-axis NC machining: a state of the art review. Comput Aided Des 51:1–17
15. Danaei B, Karbasizadeh N, Masouleh TM (2017) A general approach on collision-free workspace determination via triangle-to-triangle intersection test. Robot Comput Integr Manuf 44:230–241
16. Gian R, Lin TW, Lin AC (2003) Planning of tool orientation for five-axis cavity machining. Int J Adv Manuf Technol 22(1–3):150–160
17. Tseng YJ, Joshi S (1991) Determining feasible tool-approach directions for machining Bezier curves and surface. Comput Aided Des 23(5):367–379
18. Jimenez P, Torras C (2003) Reducing feasible contacts between polyhedral models to red–blue intersections on the sphere. Comput Aided Des 35(7):693–705
19. Jun CS, Cha K, Lee YS (2003) Optimizing tool orientations for five-axis machining by configuration-space search method. Comput Aided Des 35(6):549–566
20. Du J, Yan XG, Tian XT (2012) The avoidance of cutter gouging in five-axis machining with a fillet-end milling cutter. Int J Adv Manuf Technol 62(1–4):89–97